Elastic and photoelastic anisotropy of solid HF at high pressure

Scott A. Lee, David A. Pinnick, S. M. Lindsay, and Roland C. Hanson
Department of Physics, Arizona State University, Tempe, Arizona 85287
(Received 14 April 1986)

We report the results of a Brillouin scattering study of the elastic and photoelastic properties of solid HF as a function of pressure up to about 120 kbar. We performed near-forward-scattering experiments in which the single-crystal samples lie in a plane bisecting the scattering angle. These measurements, made in a miniature Merrill-Bassett diamond-anvil cell, yield the velocities of longitudinal- and transverse-acoustic phonons propagating along the b and a axes of single crystals of orthorhombic HF. Relative magnitudes of the elastic constants c_{11}, c_{22}, c_{44}, and c_{66} are given as a function of pressure. We have also measured the velocity of the quasilongitudinal phonon propagating in the b-a plane as a function of angle at 25.4 kbar. This measurement determines the relative magnitude of c_{12}. The values of c_{11}/ρ, c_{22}/ρ, c_{12}/ρ, c_{44}/ρ, and c_{66}/ρ at 25.4 kbar (in units of 10^{10} cm^2/sec^2) are 15.1, 28.5, 12.0, 9.74, and 2.56, respectively. We estimate the pressure dependence of the ratios of the squares of certain photoelastic constants from the intensity of the Brillouin peaks. Our results show that the polarizability derivatives associated with the shearing motion of chains of HF (and, consequently, the hydrogen bonds) are much larger than the polarizability derivatives associated with the compressional motion of the chains (and the hydrogen bonds). Both the elastic and photoelastic properties are quite anisotropic at low pressures, becoming more isotropic at higher pressure.

I. INTRODUCTION

The effects of high pressure upon hydrogen-bonded solids have been the subject of recent interest.[1,2] The two classic hydrogen-bonded solids are H_2O and HF. H_2O ice has been studied for many years. Polycrystalline solid HF has been studied[3–6] at ambient pressure. However, no studies have yet been reported on the properties of HF either in the form of single-crystal samples, or as a function of pressure. In this paper we report the results of a room-temperature Brillouin scattering study of the elastic and photoelastic properties of single crystals of solid HF up to about 120 kbar. Such data provide important information about the microscopic interactions of this molecular solid.

At low pressures, HF forms a quasi-one-dimensional solid consisting of parallel zig-zag chains of hydrogen-bonded molecules in a base-centered orthorhombic lattice ($Bm2_1b$),[5–7] where the chain axis is the b axis (Fig. 1). We have measured the velocity of longitudinal-acoustic (LA) phonons propagating parallel to the b and a axes as a function of pressure, using a method which does not require knowledge of the indices of refraction of this biaxial material (discussed below). We have also observed transverse-acoustic (TA) phonons propagating nearly parallel to the b and a axes over the same pressure range. These measurements yield the ratios of the elastic constants c_{11}, c_{22}, c_{44}, and c_{66} at each pressure and show that the degree of anisotropy of solid HF, quite large at low pressures, decreases as the pressure is increased. Our data can be used to evaluate the absolute values of these elastic constants as soon as the density of HF has been measured as a function of pressure. We have also observed quasilongitudinal phonons propagating in different directions in the b-a plane at 25.4 kbar. These measurements permit one to infer the magnitude of c_{12} relative to the other measured elastic constants at this pressure. Our observations of the intensity of the light scattered by both the LA and TA phonons propagating along the b and a axes yield information about the ratios of the squares of the appropriate photoelastic constants and their pressure

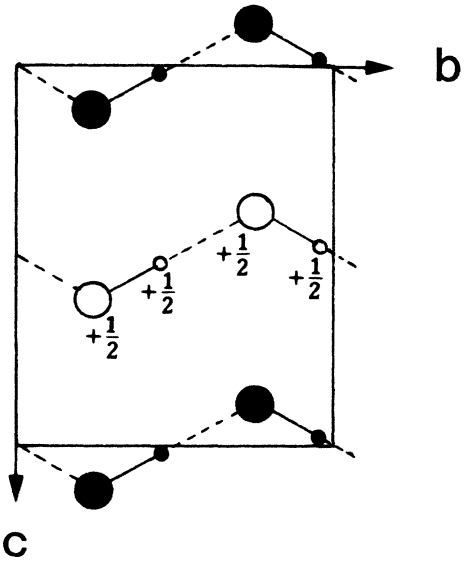

FIG. 1. Base-centered orthorhombic ($Bm2_1b$ or C_{2v}^{12}) crystal structure of solid HF at low pressures. The HF molecules form parallel zig-zag chains along the b axis. The large circles represent fluorine atoms and the small circles represent hydrogen atoms. The solid circles are atoms at $a=0$ and the open circles are atoms at $a=+\frac{1}{2}$. The a axis points into the page.

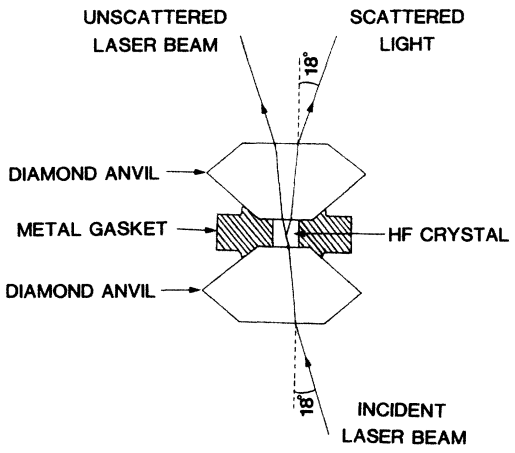

FIG. 2. Schematic diagram of the near-forward-scattering geometry used in these experiments. The single crystal of HF is contained in a hole drilled in a platinum-lined Inconel 750X gasket and pressure is applied by the diamond anvils. Note that the wave vector of the phonons probed in this equal-angle geometry is parallel to the diamond culets.

dependences. However, stress-induced birefringence in the diamonds limits the accuracy of such intensity measurements.

We have used diamond-anvil cells[8] (DAC's) in order to grow single crystals of HF and attain high pressures. Brillouin scattering is an ideal probe to use for the measurement of the elastic properties of a sample in a DAC. For these experiments we have employed a modification of the miniature Merrill-Bassett DAC which allows us to probe phonons propagating in *any* direction parallel to the diamond culet faces (Fig. 2). Previous Brillouin scattering experiments[9–13] from samples in DAC's have been limited to a few special geometries, usually backscattering. Special DAC's have been constructed with several holes drilled through the cell in order to permit several angles of scattering. The main disadvantage of such cells is that the excitations probed in such experiments are limited to only a very few crystallographic directions. Our forward-scattering geometry circumvents that limitation. However, these experiments must be performed in a miniature Merrill-Bassett DAC.

The pressure range of these experiments was limited by the fracturing of the single-crystal HF samples. This tendency to fracture may be caused by the extreme anisotropy of the elastic properties of crystalline HF. We have seen no evidence of any other phases of HF in the pressure range of these experiments. Our highest pressure is well below the transition to the expected symmetric hydrogen-bond phase,[14] and no anomalies associated with such a transition (or nonlinear excitations which may precede it) were observed.

II. EXPERIMENT

A Merrill-Bassett DAC was constructed with either hardened steel or beryllium backing plates. In order to perform our experiments in the near-forward-scattering geometry, we modified the design of the DAC by enlarging the half-angle of the cones which permit optical access to 20°. The size of the hole in contact with the diamond table was chosen to match the external aperature to the aperature of the diamond.

Samples of solid HF were loaded at liquid-nitrogen temperature into the gasket hole of a partially disassembled DAC. The cell was then assembled and warmed to room temperature. The subsequent crystal growth took place from the liquid phase of HF. Platinum-lined Inconel 750X gaskets were used to minimize the reaction between the gasket material and liquid HF.

After the HF was loaded, both the pressure and temperature of the cell was adjusted until a single-seed crystal was obtained (observed with crossed polaroids). The seed growth was anisotropic: growing first along the *b* axis, then forming a thin layer filling the hole in the gasket material, and, finally, growing normal to the diamond culet faces. The final growth phase was inferred from the observation of many interference color orders during growth. Single-crystal x-ray-diffraction studies[7] show that the crystals grow in an orientation with the *b* and *a* axes parallel to the culet faces and that the *b* axis (chain direction) is the direction in which the crystals grow initially, as observed optically. The orientation of the *b* and *a* axes relative to the DAC for all of the samples used in this study was determined by examining the sample between crossed polaroids and correlating these observations to the original growth and (in a few cases) the x-ray orientation matrix.

The melting pressure of HF at ambient temperature was measured as 14.5 kbar. The pressure range of these experiments was limited by the fracturing of the crystals at about 120 kbar. As the pressure of the cell was raised, the hole in the gasket became elliptical with the major axis of the ellipse in the *b* direction. Cracks at approximately 45° to the crystal axes appeared, presumably due to the maximum shear stress in those directions. At the

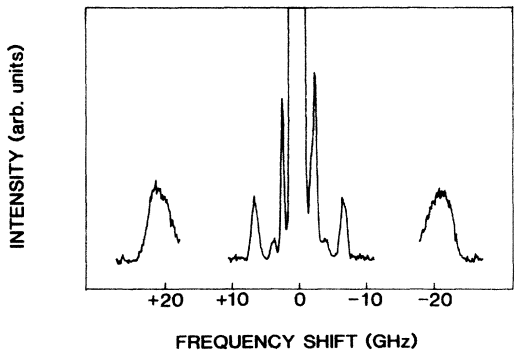

FIG. 3. Brillouin spectrum obtained for phonons propagating along the *b* axis of the HF crystal at 45.5 kbar. The LA phonon of the HF crystal occurs at 6.59 GHz, the FTA phonon occurs at 3.89 GHz, and the STA phonon occurs at 2.38 GHz. The diamond LA phonon is observed at 21.2 GHz. The Rayleigh "ghosts," appearing at 15 GHz, have been removed for clarity. The incident laser power was approximately 50 mW at a wavelength of 5145 Å.

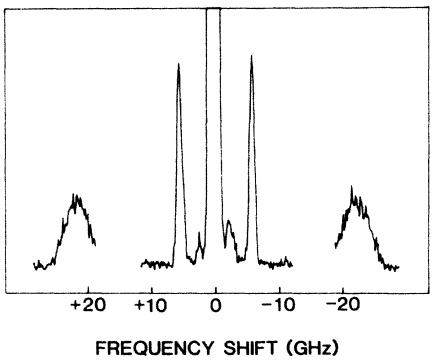

IG. 4. Brillouin spectrum obtained for phonons propagating along the a axis of the HF crystal at 45.5 kbar. The LA phonon of the HF crystal occurs at 5.48 GHz, and the TA phonon occurs at 2.30 GHz. The diamond LA phonon is observed at 20.9 GHz. The Rayleigh "ghosts," appearing at 15 GHz, have been removed for clarity. The incident laser power was approximately 50 mW at a wavelength of 5145 Å.

highest pressures these cracks became quite numerous and prevented any further light-scattering experiments.

A near-forward-scattering geometry was used in these room-temperature experiments, as shown in Fig. 2. The wave vector of the excitations probed in this geometry is parallel to the diamond culets. The supports of our DAC allowed a 20° deviation from the normal to the diamond culet faces for both the incident and scattered beams. In a typical experiment, the deviation of both the incident and scattered beams was about 18°. By rotating the DAC, we could probe any direction parallel to the culets (i.e., in the b-a plane).

We used about 50 mW of the 5145-Å line of an Ar^+-ion laser and analyzed the scattered light using a 5+4 passed tandem Fabry-Perot interferometer.[15] The high contrast of this interferometer is essential in order to measure the Brillouin spectra of these samples in this scattering geometry. Typical Brillouin spectra are shown in Figs. 3 and 4.

III. RESULTS AND DISCUSSION

Brillouin light scattering is the scattering of light by the creation or annihilation of an acoustic phonon. For the case of an optically isotropic material, the velocity, V_s, of the phonon is related to the frequency shift of the scattered light, $\Delta\nu$, the wavelength of the incident laser light, λ_i, the index of refraction n, and the scattering angle θ, via the well-known Brillouin equation

$$V_s = \frac{\lambda_i \Delta\nu}{2n \sin(\theta/2)} . \tag{1}$$

Because solid HF has orthorhombic crystal symmetry, our samples are biaxial. This complicates the interpretation of our data. The equation for Brillouin scattering[16] in an arbitrary direction in uniaxial and biaxial crystals is

$$V_s = \frac{\lambda_i \Delta\nu}{(n_{\rm in}^2 + n_{\rm sc}^2 - 2n_{\rm in}n_{\rm sc}\cos\theta)^{1/2}} , \tag{2}$$

where $n_{\rm in}$ and $n_{\rm sc}$ are the indices of refraction for the incident and scattered light, respectively.

The experiments that we report here involve three different sets of conditions. First, one set of observations involves Brillouin scattering by LA phonons propagating along either the b or a axis. For these observations, the polarization of the incident and scattered light is the same (usually perpendicular to the scattering plane) and the orthorhombic symmetry of the crystals implies that the polarization is parallel to one of the crystalline axes (which are the principal axes of the dielectric quadric). Thus, both the incident and scattered photons experience the same refraction, and Eq. (1) can be used. For our equal-angle scattering geometry, Snell's law for the wave vectors of the incident and scattered light can then be used to express Eq. (1) in terms of ψ, the external scattering angle, independent of the appropriate index of refraction of solid HF:

$$V_s = \frac{\lambda_i \Delta\nu}{2\sin(\psi/2)} . \tag{3}$$

In this manner, we have measured the velocities of the LA phonons propagating along the b and a axes, independent of the indices of refraction. As a check, we performed additional experiments with the incident light polarized in the scattering plane. The results of experiments under both polarization conditions were identical.

The second set of conditions involves Brillouin scattering by TA phonons propagating nearly parallel to either the b or a axis (within 1°, as discussed later). The incident light is polarized along a principal axis, and the scattered light will be polarized perpendicular to the incident light. Since the wave vector of both the incident and scattered light is approximately 13° from a crystallographic axis, the polarization of the scattered light will not be exactly along a principal axis. The scattered light should form two beams in the crystal (each beam given by the projection of the polarization of the scattered light onto the appropriate principal axis), and two Brillouin peaks should be observed from each TA phonon. However, in all of our spectra (made under several different polarization conditions) we observed only one peak for each transverse mode, indicating that such splitting is negligible for our experimental conditions.

The remaining group of experiments involves Brillouin scattering by the creation or annihilation of quasilongitudinal phonons propagating in an arbitrary direction in the b-a plane. For these experiments, both the incident and scattered light will be split into two beams (once again, each beam given by the projection of the polarization of the scattered light onto the appropriate principal axis). We observe only one peak for this mode, indicating that the splitting is again negligible for our experimental conditions.

We estimate the indices of refraction of solid HF at 14.5 kbar by using the measured lattice parameters of VonDreele *et al.*[7] and the Lorentz-Lorenz formula for an anisotropic crystal,[17]

$$\frac{n_i^2 - 1}{\bar{n}^2 - 1} = \frac{4\pi}{3} N\alpha_i , \tag{4}$$

TABLE I. The relationship between the velocity, the elastic constants, and the density for several different phonons in an orthorhombic crystal. (QLA denotes quasilongitudinal acoustic.)

Phonon	Expression for velocity
b-axis LA	$\sqrt{c_{22}/\rho}$
b-axis FTA	$\sqrt{c_{44}/\rho}$
b-axis STA	$\sqrt{c_{66}/\rho}$
a-axis LA	$\sqrt{c_{11}/\rho}$
a-axis TA	$\sqrt{c_{66}/\rho}$
(b-a)-plane QLA	$\left[\frac{1}{\rho}\left[\frac{c_{11}\sin^2\theta+c_{22}\cos^2\theta+c_{66}}{2}+\frac{1}{2}[(c_{11}\sin^2\theta-c_{22}\cos^2\theta)^2+2c_{66}\cos(2\theta)\times(c_{11}\sin^2\theta-c_{22}\cos^2\theta)+c_{66}^2+4c_{12}(c_{12}+2c_{66})(\cos\theta\sin\theta)^2]^{1/2}\right]\right]^{1/2}$ where θ is measured relative to the b axis

where α_i is the polarizability component corresponding to the principal index of refraction n_i, $\bar{n}^2=\frac{1}{3}(n_a^2+n_b^2+n_c^2)$, and N is the number density. In order to evaluate the α_i's we use the reported value for the average polarizability[18] ($\langle\alpha\rangle=0.84$ Å^3) and the polarizability anisotropy[19] ($\Delta\alpha=0.22$ Å^3) of molecular HF. Using these polarizabilities with the crystal-structure data yields $\alpha_a=0.767$ Å^3, $\alpha_b=0.932$ Å^3, and $\alpha_c=0.822$ Å^3. Using these values in Eq. (4), an iterative method gives $n_a=1.30$, $n_b=1.36$, and $n_c=1.32$ at 14.5 kbar. From these results we estimate the angle of propagation of the photons and phonons involved in the Brillouin scattering. In this manner we have determined that the TA phonons which we report here propagate at an angle of less than 1° from either the b or a axes. We also find that the light propagates at about 13° to the crystalline axes for the experiments probing the b- and a-axis phonons. In addition, we also use these indices of refraction with Eq. (2) in order to test the accuracy of using Eq. (3) to calculate the velocities of the transverse phonons. We find that the difference between these two calculations is only 1% at low pressure. As we shall see, solid HF becomes more isotropic at higher pressure. Consequently, we expect that this rather small difference diminishes as the pressure is increased. Consequently, we will use Eq. (3) to calculate the velocities of the TA phonons over the entire pressure range of these experiments.

The velocities of the phonons probed in these experiments are determined by the elastic constants[20] as listed in Table I. The velocities of the longitudinal- and transverse-acoustic phonons propagating along the b and a axes are determined by only one elastic constant, making the determination of these elastic constants unambiguous. For our results, only c_{12} is determined from an equation involving more than one elastic constant, and we discuss this case later.

In Fig. 3 we show a typical Brillouin spectrum for phonons propagating along the b axis at 45.5 kbar. The incident light is polarized along the a axis. In this spectrum we observe a peak corresponding to a LA phonon and two peaks corresponding to TA phonons. This identification of the peaks has been confirmed by studying the polarization of the scattered light. We shall refer to the two TA peaks as "STA" (for slow transverse acoustic) and "FTA" (for fast transverse acoustic), where the STA phonon has a smaller frequency shift than the FTA phonon. Group-theory arguments for Brillouin scattering in optically anisotropic materials[16,21,22] show that light scattering is allowed only for the TA phonon propagating along the b axis with displacement pattern $u=(1,0,0)$ for our experimental conditions. We identify the STA phonon as that TA phonon since the intensity of light scattered by the STA phonon is much greater than the intensity of light scattered by the FTA phonon. The observation of the FTA phonon is attributed to the unavoidable amount of depolarization of the incident light caused by stress-induced birefringence in the diamonds of the DAC.

In Fig. 4 we show a typical Brillouin spectrum for phonons propagating along the a axis at 45.5 kbar. We observe a rather weak Brillouin signal for only one of the TA phonons, as predicted by group theory. Both of the TA phonons propagating along the b and a axes with nonzero Brillouin light-scattering tensor elements have the same elastic constant, c_{66}, and hence the same velocity. Our experiments find that the STA phonon observed along the b axis and the TA phonon observed along the a axis propagate with the same velocity at each pressure, confirming our identification of the STA phonon of the b axis as the $u=(1,0,0)$ phonon. However, the intensities of the light scattered by these two TA phonons (the b-axis STA and the a-axis TA) are quite different.

In Fig. 5 we show the pressure dependence of the velocity of the LA phonons propagating parallel to the b and a axes. The circles are the experimentally measured phonon velocities along the b axis, the triangles are the experimentally measured phonon velocities along the a axis, and the solid lines are regression fits to the experimental data. The coefficients for these fits are given in Table II.

Small errors in the scattering angle give rise to relative-

TABLE II. The regression-fit parameters for the pressure dependence of the velocity of several different phonons of solid HF up to 120 kbar. The velocity is given as $V=(a+bP+cP^2)\times 10^5$ cm/sec, where the pressure is measured in kbar.

Phonon	a	b	c (10^{-4})
b-axis LA	4.11±0.23	0.0496±0.0083	−1.94±0.63
b-axis FTA	2.03±0.12	0.0387±0.0044	−1.67±0.33
a-axis LA	2.52±0.19	0.0663±0.0076	−3.59±0.66
b-axis STA and a-axis TA	1.28±0.07	0.0170±0.0015	0.0

ly large errors in the velocities because of the small scattering angle of our near-forward-scattering geometry. This causes the observed spread in the experimental data. The fact that the data for phonons propagating perpendicular to the b axis for our four successful experimental runs all lie on the same curve confirms that the orientation of our single crystals were the same in the four samples.

From our regression fits, we determine that the ratio of the velocities of the longitudinal phonons propagating along the b and a axes at atmospheric pressure is approximately 1.63. This implies that the ratio of the elastic constants c_{22}/c_{11} is 2.7, a relatively large anisotropy.

The chains consist of alternating covalent and hydrogen bonds (Fig. 1). Neighboring chains are held together by dipolar and van der Waals forces. Consequently, the speed of sound is much greater along the chains (the b axis) than perpendicular to the chains, as can be seen in Fig. 5. As the pressure is raised, the lattice parameters along the a and c directions decrease by a relatively larger amount than the b lattice parameter decreases. This is due to the fact that the interchain forces are much less stiff than the covalent and hydrogen bonds. Thus, due to anharmonicity, the strengths of the interactions in the a and c directions change by an amount which is relatively larger than the change for the b direction. In this manner, the degree of anisotropy decreases as the pressure is increased. This decrease in the anisotropy can be seen in Fig. 5. At 100 kbar the ratio of the longitudinal velocities is about 1.28 and the ratio of the corresponding elastic constants is 1.6.

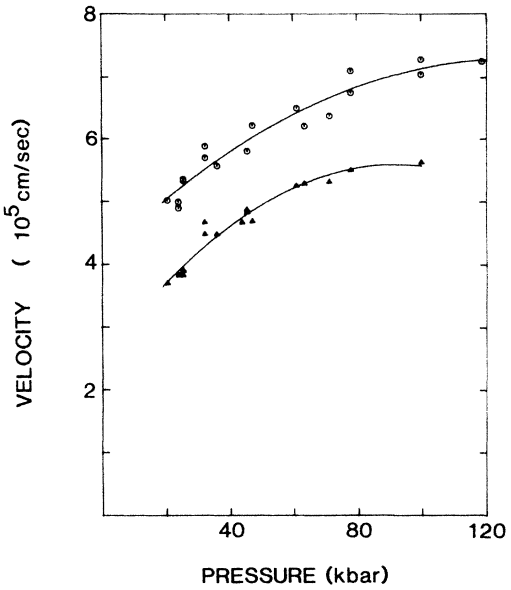

FIG. 5. The pressure dependence of the velocity of LA phonons propagating along the b and a axes. The open circles represent the data for the b-axis LA phonons and the triangles represent the data for the a-axis LA phonons. The solid lines are regression fits to the data. The coefficients for these fits are given in Table II.

Figure 6 shows the results for the transverse phonons propagating parallel to the b and a axes. As stated earlier, light scattered by transverse phonons has a different polarization from the incident light. Consequently, the near-forward-scattering geometry does not measure the velocity of the transverse phonons independent of the indices of refraction. However, as we saw earlier, the error introduced by using Eq. (3) for the TA data is quite small. In Fig. 6 we show the measured velocity as a function of pressure using Eq. (3). We have observed two transverse-acoustic phonons (the STA and FTA) propagating nearly parallel to the b axis and one transverse-acoustic (the TA) phonon propagating nearly parallel to the a axis. The solid lines are regression fits to the data and the coefficients are given in Table II.

We have measured the velocity of quasilongitudinal phonons as a function of angle in the b-a plane at 25.4 kbar. The velocity of this mode (given in Table I) is

$$V=\left[\frac{1}{\rho}\left[\frac{c_{11}\sin^2\theta+c_{22}\cos^2\theta+c_{66}}{2}+\tfrac{1}{2}[(c_{11}\sin^2\theta-c_{22}\cos^2\theta)^2+2c_{66}(c_{11}\sin^2\theta-c_{22}\cos^2\theta)\cos 2\theta+c_{66}^2+4c_{12}(c_{12}+2c_{66})(\cos\theta\sin\theta)^2]^{1/2}\right]\right]^{1/2}, \quad (5)$$

where θ is measured with respect to the b axis. From the spectra for the b and a axes we determine c_{11}, c_{22}, and c_{66} (to within a multiplicative constant since we do not know ρ). By fitting our data to Eq. (5), we determine the relative size of c_{12}. Our relative values of the five elastic constants measured at 25.4 kbar (also including c_{44}) are given in Table III. The solid line in Fig. 7 is Eq. (5) and the circles are our experimental data.

We have also observed quasitransverse phonons propagating in the b-a plane. However, the number of such

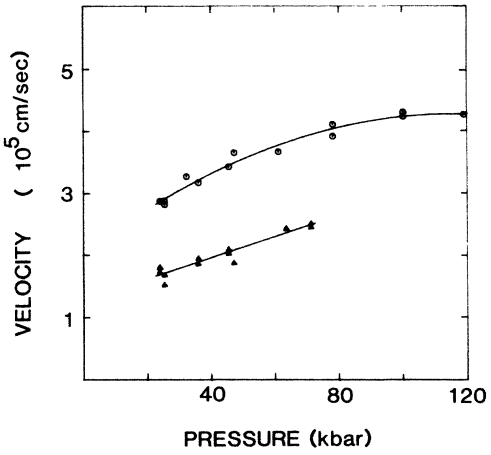

FIG. 6. The pressure dependence of the velocity of TA phonons propagating along the b and a axes. The open circles represent the data for the b-axis FTA phonons and the triangles represent the data for the b-axis STA and a-axis TA phonons (which have the same velocities). The solid lines are regression fits to the data. The coefficients for these fits are given in Table II.

Brillouin peaks and their associated frequency shifts changed for different polarization conditions of the incident light. This prevented an unambiguous identification of the associated modes, and we will not discuss these observations further.

As mentioned earlier, stress-induced birefringence in the diamonds of the DAC causes polarization scrambling of both the incident and scattered light. This introduces significant errors into the intensity measurements of the observed light scattering. Group-theory arguments[16] show that the intensity of the light scattered for each phonon is proportional to the square of only one photoelastic

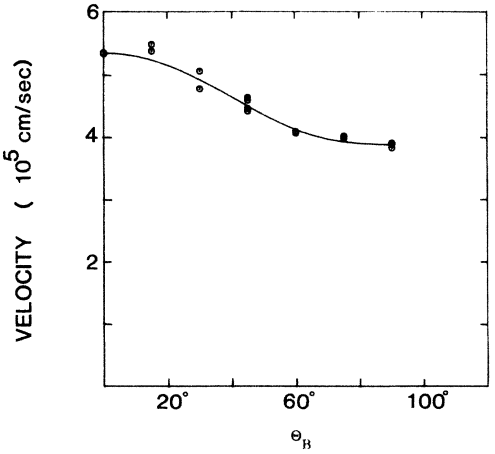

FIG. 7. The angular dependence of the velocity of the quasi-longitudinal phonon propagating in the b-a plane. The open circles represent the data and the solid line is Eq. (5) with $c_{11}/\rho = 1.51\times10^{11}$ cm^2/sec^2, $c_{22}/\rho = 2.85\times10^{11}$ cm^2/sec^2, $c_{12}/\rho = 1.20\times10^{11}$ cm^2/sec^2, $c_{44}/\rho = 9.74\times10^{10}$ cm^2/sec^2, and $c_{66}/\rho = 2.56\times10^{10}$ cm^2/sec^2.

TABLE III. The values of our measured elastic constants (divided by the density) for solid HF at 25.4 kbar.

Elastic constant / ρ	Value (10^{10} cm^2/sec^2)
c_{11}/ρ	15.1
c_{22}/ρ	28.5
c_{12}/ρ	12.0
c_{44}/ρ	9.74
c_{66}/ρ	2.56

constant for the spectra obtained for LA and (in our geometry) TA phonons propagating along the b and a axes. We display in Table IV the pressure dependences of the ratios of the squares of the appropriate photoelastic constants of HF. We see that the ratio $(p'_{1212}/p'_{1122})^2$ (the photoelastic constants appropriate for the STA and LA phonons propagating along the b axis) is roughly independent of pressure and that the ratio $(p'_{1221}/p'_{2211})^2$ (the photoelastic constants appropriate for the TA and LA phonons propagating along the a axis) increases with pressure. We also find that the ratio $(p'_{1212}/p'_{1122})^2$ is roughly 16 times larger than the ratio of $(p'_{1221}/p'_{2211})^2$ at 24.0 kbar. In fact, by comparing Figs. 3 and 4 we see that these two ratios are still quite different at 45.5 kbar. Recalling that the displacement vector for the b-axis STA phonon is $u=(1,0,0)$, our results show that the polarizability derivative associated with shearing motion of the chains (and, consequently, the hydrogen bonds) is much larger than the polarizability derivative associated with the compressional motion of the chains (and the hydrogen bonds).

In Table V we display the ratio of the intensity of the light scattered by the HF phonons to the intensity of light scattered by a diamond (longitudinal) mode. From these results, we estimate the pressure dependence of the squares of the photoelastic constants themselves by assuming that the change in this ratio of intensities reflects a change primarily in the HF photoelastic constants. In order to avoid any complications caused by different orientations between the crystalline axes of diamonds and the HF single crystals, we have listed data from only one experimental run (i.e., one crystal of HF). These data show that the square of the HF photoelastic constants decrease by more than an order of magnitude over the pres-

TABLE IV. The pressure dependence of the ratio of the squares of our measured photoelastic constants of solid HF as a function of pressure.

P (kbar)	$\left[\frac{p'_{1212}}{p'_{1122}}\right]^2$	$\left[\frac{p'_{1221}}{p'_{2211}}\right]^2$	$\frac{(p'_{1212}/p'_{1122})^2}{(p'_{1221}/p'_{2211})^2}$
24.0	0.14	0.009	16
36.0	0.17	0.017	10
45.5	0.19	0.019	10
63.5	0.14	0.025	5.6
71.5	0.17	0.046	3.7

TABLE V. The pressure dependence of the ratio of the intensity of the light scattered by a particular HF phonon to the intensity scattered by the diamond LA mode.

P (kbar)	$\frac{I_{LA}(b \text{ axis})}{I_D \sim (p'_{1122})^2}$	$\frac{I_{STA}(b \text{ axis})}{I_D \sim (p'_{1212})^2}$	$\frac{I_{LA}(a \text{ axis})}{I_D \sim (p'_{2211})^2}$	$\frac{I_{TA}(a \text{ axis})}{I_D \sim (p'_{1221})^2}$
24.0	0.60	0.78	1.00	0.04
36.0	0.61	0.96	0.57	0.05
45.5	0.24	0.40	0.67	0.05
63.5	0.07	0.07	0.34	0.03
71.3	0.05	0.07	0.09	0.02

sure range of our experiments. This illustrates the decrease in the electronic polarizability derivative as the volume available to the electrons is decreased. The decrease of $(p'_{1221})^2$ appears to be smaller, only about a factor of 2, but the errors inherent in measuring this small photoelastic constant are large. At the lowest pressures, Table V shows (as can also be seen by comparing the spectra in Figs. 3 and 4) that $(p'_{2211})^2$ is larger than $(p'_{1122})^2$, by approximately a factor of 2. More dramatically, $(p'_{1212})^2$ is roughly an order of magnitude larger than $(p'_{1221})^2$.

IV. CONCLUSIONS

We have presented the results of a room-temperature Brillouin scattering study of solid HF as a function of pressure. We performed these experiments by using a modification of the miniature Merrill-Bassett DAC, which permitted the use of a near-forward-scattering geometry. The equal-angle nature of this scattering geometry permitted the direct measurement of the velocities of certain acoustic phonons independent of the indices of refraction. The forward-scattering nature of our scattering geometry permitted the routine observation of Brillouin scattering from TA phonons, using the tandem interferometer. The observation of the TA phonons along the crystalline axes allowed us to provide information about the related elastic constants in an unambiguous manner.

We have measured the pressure dependence of the velocity of LA and TA phonons propagating along the b and a axes. Along the crystalline axes, the velocities of the LA and TA phonons are determined by only one elastic constant for our orthorhombic material. Our measurements provide the ratios of the appropriate elastic constants (c_{11}, c_{22}, c_{44}, c_{66}) at each pressure, and can be converted to absolute elastic constants when the pressure dependence of the density becomes available. We have also measured the velocity of quasilongitudinal phonons propagating in many directions in the b-a plane at 25.4 kbar which permits us to evaluate the relative size of c_{12}. Our measurements show that the elastic properties of HF are quite anisotropic at low pressures and become more isotropic as the applied pressure is increased.

We find that the photoelastic properties are also quite anisotropic at low pressures. Our results indicate that the photoelastic constants (and, hence, the polarizability derivatives) associated with a shearing motion of the chains (and the hydrogen bonds) are significantly larger than the photoelastic constants associated with a compressional motion of the chains (and hydrogen bonds). The degree of the photoelastic anisotropy decreases as the pressure is increased.

In conclusion, we have found solid HF at high pressures to be a highly anisotropic material with many interesting properties. We hope that these experimental data will stimulate theoretical work.

ACKNOWLEDGMENT

One of us (S.A.L.) was supported by the U.S. Office of Naval Research (ONR) under Contract No. N00014-84-C-048.

[1]K. R. Hirsch and W. B. Holzapfel, Phys. Lett. **101A**, 142 (1984).
[2]A. Polian and M. Grimsditch, Phys. Rev. Lett. **52**, 1312 (1984).
[3]J. S. Kittelberger and D. F. Hornig, J. Chem. Phys. **46**, 3099 (1967).
[4]A. Anderson, B. H. Torrie, and W. S. Tse, Chem. Phys. Lett. **70**, 300 (1980).
[5]M. W. Johnson, E. Sandor, and E. Arzi, Acta Crytallogr., Sect. B **31**, 1998 (1975).
[6]M. Atoji and W. N. Lipscomb, Acta Crystallogr. **7**, 173 (1954).
[7]R. VonDreele, D. A. Pinnick, and R. C. Hanson (unpublished).
[8]A. Jayaraman, Rev. Mod. Phys. **55**, 65 (1983).
[9]C. H. Whitfield, E. M. Brody, and W. A. Bassett, Rev. Sci. Instrum. **47**, 942 (1976).
[10]W. A. Bassett, D. R. Wilbrun, J. A. Hrubec, and E. M. Brody, in *High Pressure Science and Technology,* edited by K. D. Timmerhaus and M. S. Barber (Plenum, New York, 1979), Vol. 2, p. 75.
[11]H. Shimizu, E. M. Brody, H. K. Mao, and P. M. Bell, Phys. Rev. Lett. **47**, 128 (1981).
[12]A. Polian, J. M. Besson, M. Grimsditch, and H. Vogt, Phys. Rev. B **25**, 2767 (1982).
[13]H. Shimizu, T. Kumazawa, E. M. Brody, H. K. Mao, and P. M. Bell, Jpn. J. Appl. Phys. **22**, 52 (1983).
[14]R. Jansen, O. F. Sankey, and R. Bertoncini (unpublished).
[15]S. M. Lindsay, M. W. Anderson, and J. R. Sandercock, Rev.

Sci. Instrum. **52**, 1476 (1981).
[16]R. Vacher and L. Boyer, Phys. Rev. B **6**, 639 (1972).
[17]M. F. Vuks, Opt. Spektrosk. **20**, 644 (1966) [Opt. Spectrosc. (USSR) **20**, 361 (1966)].
[18]A. J. Perkins, J. Phys. Chem. **68**, 654 (1964).
[19]J. S. Muenter, J. Chem. Phys. **56**, 5409 (1972).
[20]R. Truell, C. Elbaum, and B. B. Chick, *Methods in Solid State Physics* (Academic, New York, 1969), Chap. 1.
[21]D. F. Nelson, P. D. Lazay, and M. Lax, Phys. Rev. B **6**, 3109 (1972).
[22]H. Z. Cummins and P. E. Schoen, in *Laser Handbook,* edited by F. T. Arrecchi and E. O. Schulz-Dubois (American Elsevier, New York, 1972), Vol. 2, p. 1029.